

# Algebraic to exponential decay of spatial correlations in one-dimensional and confined hard-core fluids: A Laplace-pole analysis

Ana M. Montero<sup>1</sup> and Andrés Santos<sup>2</sup>

<sup>1</sup>*Departamento de Física, Universidad de Extremadura, E-06006 Badajoz, Spain*

<sup>2</sup>*Departamento de Física and Instituto de Computación Científica Avanzada (ICCAEX), Universidad de Extremadura, E-06006 Badajoz, Spain*

(Dated: December 4, 2025)

We derive the asymptotic behavior of the radial distribution function  $g(x)$  for one-dimensional (1D) hard-rod systems and related quasi-one-dimensional geometries at high packing fractions using Laplace transform techniques and pole analysis. By identifying the poles and residues of the Laplace transform in the limit of small void fraction, we obtain compact representations of  $g(x)$  in terms of the Jacobi elliptic theta function  $\theta_3$ . This formulation naturally captures the two regimes governing the oscillatory decay toward unity: an intermediate algebraic decay and a long-distance exponential decay, consistent with previous results for the Tonks gas. Our approach provides a unified framework that (i) expresses  $g(x)$  in a single well-tabulated special function, (ii) links spatial correlations directly to the pole structure in complex Laplace space, offering clear physical insight into decay rates and oscillation frequencies, and (iii) generalizes straightforwardly to 1D binary mixtures and confined hard-disk systems, where direct Gaussian decompositions are cumbersome. The equivalence between the theta-function representation and the Gaussian superposition of Bouzar and Messina [Phys. Rev. E **112**, L042105 (2025)] is established via the Poisson summation formula, highlighting the versatility and conceptual advantages of the Laplace-pole framework.

## I. INTRODUCTION

In a recent paper [1], Bouzar and Messina revisited the exact radial distribution function (RDF)  $g(x)$  of the one-dimensional (1D) hard-rod fluid (Tonks gas) [2, 3]. Although the Tonks gas is a well-known and extensively studied system, their work revealed noteworthy findings. This underscores that, despite its apparent simplicity, the system remains relevant both theoretically, through the identification of previously unrecognized features, and practically, as the 1D polydisperse hard-rod model has recently been used to explore the behavior of hard disks and hard spheres under single-file confinement [4, 5].

In particular, Bouzar and Messina showed that, when the packing fraction  $\phi$  is sufficiently close to its close-packing value  $\phi_{\text{cp}} = 1$ , the oscillatory decay of  $g(x)$  exhibits two distinct regimes: (i) for  $(x-1)\phi \lesssim 0.077/\bar{\phi}^2$ , the decay is algebraic with an envelope  $g^{\text{env}}(x) \sim (x-1)^{-1/2}$ , whereas (ii) for  $(x-1)\phi \gtrsim 0.077/\bar{\phi}^2$ , the decay is exponential with an envelope  $g^{\text{env}}(x) - 1 \sim e^{-\kappa x}$ . Here the rod length is taken as the unit of length,  $\bar{\phi} \equiv 1 - \phi$  denotes the void fraction, and  $\kappa = 2\pi^2\phi\bar{\phi}^2$  is the damping coefficient. The algebraic regime (i) indicates an emerging crystallization, which is eventually frustrated by the exponential regime (ii), except in the limiting case  $\phi \rightarrow \phi_{\text{cp}}$ .

In their analysis, Bouzar and Messina introduced the scaled variable

$$\tilde{x} = (x-1)\phi \quad (1)$$

and showed that, for sufficiently small  $\bar{\phi}$ ,  $g(x)$  can be

approximated by

$$\tilde{g}(\tilde{x}) \equiv g(x) \approx \bar{\phi}^{-1} \sum_{n=-\infty}^{\infty} \frac{e^{-(\tilde{x}-n)^2/2\bar{\phi}^2|n|}}{\sqrt{2\pi|n|}}, \quad (2)$$

which has local maxima at  $\tilde{x} = \text{integer}$ , with an envelope

$$\tilde{g}^{\text{env}}(\tilde{x}) = \theta_3\left(0, e^{-2\pi^2\bar{\phi}^2\tilde{x}}\right), \quad (3)$$

where

$$\begin{aligned} \theta_3(z, q) &= \sum_{n=-\infty}^{\infty} q^{n^2} e^{2inz} \\ &= 1 + 2 \sum_{n=1}^{\infty} q^{n^2} \cos(2nz), \quad |q| < 1, \end{aligned} \quad (4)$$

is the Jacobi elliptic theta function [6, (20.2.3)]. Taking into account its mathematical properties

$$\theta_3(0, q) \simeq \begin{cases} \sqrt{\frac{\pi}{\ln q^{-1}}}, & 0.217 \lesssim q < 1, \\ 1 + 2q, & 0 \leq q \lesssim 0.217, \end{cases} \quad (5)$$

the two regimes (i) and (ii) follow directly as

$$\tilde{g}^{\text{env}}(\tilde{x}) \simeq \begin{cases} \frac{1}{\sqrt{2\pi\bar{\phi}^2\tilde{x}}}, & \tilde{x} \lesssim \frac{0.077}{\bar{\phi}^2} \\ 1 + 2e^{-2\pi^2\bar{\phi}^2\tilde{x}}, & \tilde{x} \gtrsim \frac{0.077}{\bar{\phi}^2}. \end{cases} \quad (6)$$

The intermediate algebraic decay in Eq. (6) had already been obtained by Hu and Charbonneau [7] through a simple physical argument.

While the Gaussian representation (2) offers valuable physical insight by decomposing the RDF into localized contributions, alternative mathematical formulations can provide complementary advantages. In statistical mechanics, different representations of the same quantity often highlight distinct aspects of the underlying physics and suggest different routes for generalization or approximation. In particular, Fourier and Laplace representations have proven especially useful in the analysis of correlation functions, as they naturally expose the characteristic frequencies and decay rates associated with spatial oscillations.

In this paper, we extend the results of Refs. [1, 7] using a Laplace transform combined with a pole analysis. This approach leads to a compact representation in terms of the Jacobi theta function  $\theta_3$ , which is practically equivalent to Eq. (2) but offers several practical and conceptual advantages: (a) it involves a single, well-tabulated special function rather than an infinite sum, (b) it directly links the spatial oscillation structure to poles in the complex frequency plane, clarifying the underlying decay mechanisms, and (c) it applies straightforwardly to related systems, including 1D mixtures and quasi-one-dimensional (q1D) geometries, where the direct Gaussian decomposition becomes algebraically cumbersome.

The paper is organized as follows. Section II presents the Laplace-transform and pole analysis for the mono-component hard-rod system (Tonks gas). The same strategy is then applied to the more general case of a symmetric nonadditive binary mixture. In Sec. IV, we move beyond strictly 1D systems and analyze the RDFs of hard disks under single-file confinement. Finally, Sec. V summarizes our conclusions.

## II. MONOCOMPONENT SYSTEM

We introduce the Laplace representation

$$G(s) = \int_0^\infty dx e^{-sx} g(x) \quad (7)$$

of  $g(x)$ . For the Tonks gas, this transform is [3]

$$G(s) = \phi^{-1} \left[ e^s \left( 1 + \frac{\bar{\phi}}{\phi} s \right) - 1 \right]^{-1}. \quad (8)$$

The Laplace transform of  $\tilde{g}(\tilde{x})$  is related to  $G(s)$  through

$$\tilde{G}(s) = \phi e^{\phi s} G(\phi s) = (1 + \bar{\phi} s - e^{-\phi s})^{-1}. \quad (9)$$

We now denote by  $\{s_n = -\zeta_n \pm i\omega_n, n = 1, 2, \dots\}$  the nonzero poles of  $\tilde{G}(s)$ . Their real and imaginary parts satisfy

$$1 - \bar{\phi}\zeta_n = e^{\phi\zeta_n} \cos(\phi\omega_n), \quad -\bar{\phi}\omega_n = e^{\phi\zeta_n} \sin(\phi\omega_n), \quad (10)$$

and the corresponding residues are

$$\begin{aligned} A_n &= \lim_{s \rightarrow s_n} (s - s_n) \tilde{G}(s) = (1 + \phi\bar{\phi}s_n)^{-1} \\ &= \frac{1 - \phi\bar{\phi}(\zeta_n \pm i\omega_n)}{(1 - \phi\bar{\phi}\zeta_n)^2 + (\phi\bar{\phi}\omega_n)^2}. \end{aligned} \quad (11)$$

Thus  $A_n = |A_n|e^{\pm i\delta_n}$ , with

$$|A_n| = \left[ (1 - \phi\bar{\phi}\zeta_n)^2 + (\phi\bar{\phi}\omega_n)^2 \right]^{-1/2}, \quad (12a)$$

$$\delta_n = \mp \tan^{-1} \frac{\phi\bar{\phi}\omega_n}{1 - \phi\bar{\phi}\zeta_n}. \quad (12b)$$

In terms of these poles and the residues,  $\tilde{g}(\tilde{x})$  admits the exact representation

$$\begin{aligned} \tilde{g}(\tilde{x}) &= 1 + \sum_{n=1}^{\infty} A_n e^{s_n \tilde{x}} \\ &= 1 + 2 \sum_{n=1}^{\infty} |A_n| e^{-\zeta_n \tilde{x}} \cos(\omega_n \tilde{x} + \delta_n). \end{aligned} \quad (13)$$

In general, the coupled equations (10) must be solved numerically. However, in the limit of small void fraction ( $\bar{\phi} \ll 1$ ), their solutions reduce to

$$\zeta_n = 2n^2 \pi^2 \bar{\phi}^2 + \mathcal{O}(\bar{\phi}^4), \quad \omega_n = 2n\pi + \mathcal{O}(\bar{\phi}^3), \quad (14a)$$

$$|A_n| = 1 + \mathcal{O}(\bar{\phi}^2), \quad \delta_n = \mathcal{O}(\bar{\phi}). \quad (14b)$$

Inserting these expressions into Eq. (13) gives

$$\begin{aligned} \tilde{g}(\tilde{x}) &\approx 1 + 2 \sum_{n=1}^{\infty} e^{-2n^2 \pi^2 \bar{\phi}^2 \tilde{x}} \cos(2n\pi \tilde{x}) \\ &= \theta_3(\pi \tilde{x}, e^{-2\pi^2 \bar{\phi}^2 \tilde{x}}), \quad \bar{\phi} \ll 1, \end{aligned} \quad (15)$$

where the second step follows from Eq. (4).

Figure 1 shows the ratios  $\zeta_n/2n^2\pi^2\bar{\phi}^2$  and  $\omega_n/2n\pi$  for  $0 \leq \bar{\phi} \leq 0.05$  for  $n = 1, 2, \dots, 10$ . As expected, the accuracy of the asymptotic expressions (14a) deteriorates as  $n$  and/or  $\bar{\phi}$  increase. Nevertheless, Eq. (15) remains remarkably accurate, as illustrated in Fig. 2.

It can be verified that the local maxima of  $\theta_3(z, e^{-az})$  occur at  $z_m \approx m\pi - \mathcal{O}(a)$ , with  $m = 0, 1, 2, \dots$ . Consequently, for small  $a$ , the envelope of  $\theta_3(z, e^{-az})$  is well approximated by  $\theta_3(0, e^{-az})$ . Thus, the representation in Eq. (15) leads to the same conclusions as those obtained by Bouzar and Messina from Eq. (2). Indeed, using the Poisson summation formula  $\sum_{n=-\infty}^{\infty} f(n) = \sum_{n=-\infty}^{\infty} \int_{-\infty}^{\infty} dx f(x) e^{-2\pi i n x}$  [6, (1.8.14)], one finds

$$\theta_3(\pi \tilde{x}, e^{-2\pi^2 \bar{\phi}^2 \tilde{x}}) = \frac{\bar{\phi}^{-1}}{\sqrt{2\pi \tilde{x}}} \sum_{n=-\infty}^{\infty} e^{-(\tilde{x}-n)^2/2\bar{\phi}^2 \tilde{x}}. \quad (16)$$

Approximating  $e^{-(\tilde{x}-n)^2/2\bar{\phi}^2 \tilde{x}}/\sqrt{2\pi \tilde{x}} \approx e^{-(\tilde{x}-n)^2/2\bar{\phi}^2 |n|}/\sqrt{2\pi |n|}$  then recovers Eq. (2) from Eqs. (15) and (16).

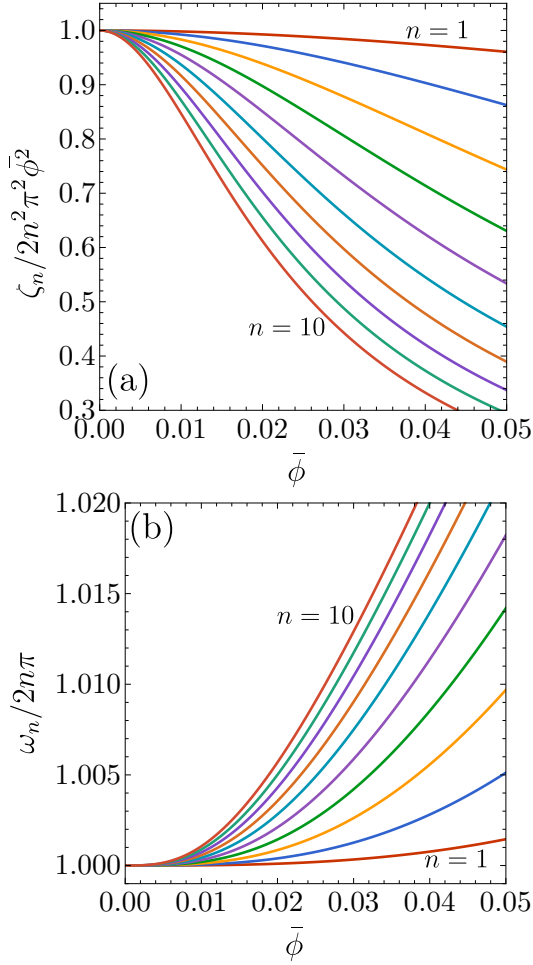


FIG. 1. Monocomponent system. (a)  $\zeta_n/2n^2\pi^2\bar{\phi}^2$  and (b)  $\omega_n/2n\pi$  as functions of  $\bar{\phi}$  for  $n = 1, 2, \dots, 10$  [from top to bottom in panel (a) and from bottom to top in panel (b)].

### III. SYMMETRIC NONADDITIVE BINARY MIXTURES

We now consider an equimolar binary hard-rod mixture with diameters  $\sigma_{11} = \sigma_{22} = 1$  and  $\sigma_{12} = a < 1$  (negative nonadditivity). It can be shown [3] that the equation of state is

$$\frac{1}{\rho} = \frac{1}{\beta p} + \frac{a + e^{-(1-a)\beta p}}{1 + e^{-(1-a)\beta p}}, \quad (17)$$

where  $\rho$  is the number density,  $\beta = 1/k_B T$  is the inverse temperature, and  $p$  is the pressure. In general,  $\beta p$  cannot be expressed explicitly as a function of  $\rho$ . However, in the high-pressure regime ( $\beta p \gg 1$ ), the equation of state gives  $\beta p a \approx \phi/\bar{\phi}$  with  $\phi = \rho a$  and  $\bar{\phi} = 1 - \phi$ .

By analogy with Eq. (1), we define

$$\tilde{x} = \left(\frac{x}{a} - 1\right)\phi \quad (18)$$

and  $\tilde{g}_{ij}(\tilde{x}) \equiv g_{ij}(x)$ . The Laplace transform of  $\tilde{g}_{ij}(\tilde{x})$  is  $\tilde{G}_{ij}(s) = (\phi/a)e^{\phi s} G_{ij}(\phi s/a)$ , where  $G_{ij}(s)$  is the Laplace

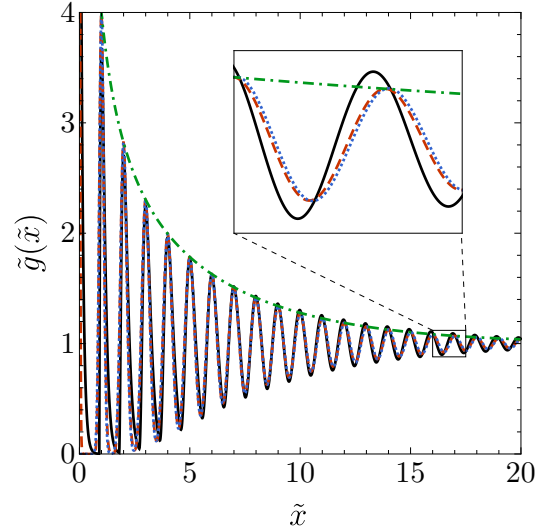


FIG. 2. Monocomponent system. Plot of  $\tilde{g}(\tilde{x})$  for  $\phi = 0.9$ . The solid, dotted, and dashed lines correspond to the exact function, the Gaussian approximation [Eq. (2)], and our approximation [Eq. (15)], respectively. The envelope [Eq. (3)] is also shown (dashed-dotted line). The dashed and dotted lines are nearly indistinguishable.

transform of  $g_{ij}(x)$  (see Appendix A). Consequently,

$$\tilde{G}_{11}(s) \approx 2 \frac{1 - \tilde{D}(s)}{\tilde{D}(s)} e^{\phi s}, \quad \tilde{G}_{12}(s) \approx \frac{2}{(1 + \bar{\phi}s)\tilde{D}(s)}, \quad (19a)$$

$$\tilde{D}(s) \approx \frac{1 + \bar{\phi}s - e^{-\phi s}}{1 + \bar{\phi}s} \frac{1 + \bar{\phi}s + e^{-\phi s}}{1 + \bar{\phi}s}. \quad (19b)$$

The poles  $\{s_n = -\zeta_n \pm i\omega_n\}$  of  $\tilde{G}_{ij}(s)$  are the roots of  $\tilde{D}(s) = 0$ , i.e.,

$$1 + \bar{\phi}s_n = \pm e^{-\phi s_n}. \quad (20)$$

Comparison with Eq. (9) shows that the roots with the + sign coincide with those of the monocomponent system,

$$\zeta_n \approx \frac{n^2 \pi^2 \bar{\phi}^2}{2}, \quad \omega_n \approx n\pi, \quad (21)$$

with  $n = 2, 4, \dots = \text{even}$ . The roots corresponding to the - sign are also given by Eq. (21), but now with  $n = 1, 3, \dots = \text{odd}$ .

The ratios  $\zeta_n/(n^2\pi^2\bar{\phi}^2/2)$  and  $\omega_n/n\pi$  for  $n = 1, 2, \dots, 10$  are shown in Fig. 3 for a binary mixture with  $a = \frac{1}{2}$ . The behavior is qualitatively similar to that of the monocomponent fluid (cf. Fig. 1), although the deviations from unity are smaller in the mixture.

To compute the residues, note that

$$\tilde{D}'(s_n) = 2 \frac{1 + \phi \bar{\phi} s_n}{1 + \bar{\phi} s_n} \approx 2. \quad (22)$$

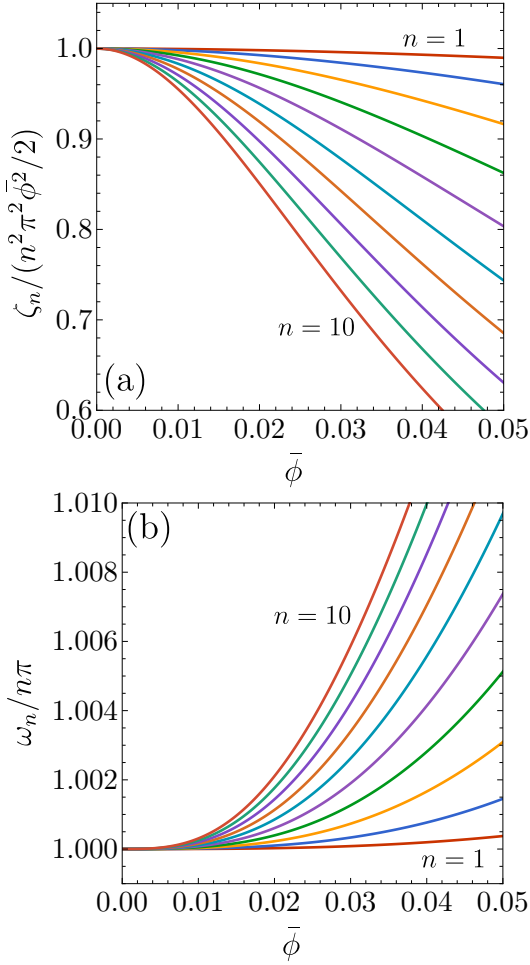


FIG. 3. Symmetric binary mixture with  $a = \frac{1}{2}$ . (a)  $\zeta_n / (n^2 \pi^2 \bar{\phi}^2 / 2)$  and (b)  $\omega_n / n\pi$  as functions of  $\bar{\phi}$  for  $n = 1, 2, \dots, 10$  [from top to bottom in panel (a) and from bottom to top in panel (b)].

Hence,

$$\lim_{s \rightarrow s_n} (s - s_n) \tilde{G}_{11}(s) = (-1)^n, \quad (23a)$$

$$\lim_{s \rightarrow s_n} (s - s_n) \tilde{G}_{12}(s) = 1. \quad (23b)$$

In Eq. (23a) we have used that  $e^{-\phi s_n} = (-1)^n (1 + \bar{\phi} s_n) \approx (-1)^n$ .

Finally, applying the residue theorem, we obtain

$$\begin{aligned} \tilde{g}_{11}(\tilde{x}) &\approx 1 + 2 \sum_{n=1}^{\infty} (-1)^n e^{-n^2 \pi^2 \bar{\phi}^2 \tilde{x} / 2} \cos(n\pi \tilde{x}) \\ &= \theta_3 \left( \frac{\pi(\tilde{x} - 1)}{2}, e^{-\pi^2 \bar{\phi}^2 \tilde{x} / 2} \right), \end{aligned} \quad (24a)$$

$$\begin{aligned} \tilde{g}_{12}(\tilde{x}) &\approx 1 + 2 \sum_{n=1}^{\infty} e^{-n^2 \pi^2 \bar{\phi}^2 \tilde{x} / 2} \cos(n\pi \tilde{x}) \\ &= \theta_3 \left( \frac{\pi \tilde{x}}{2}, e^{-\pi^2 \bar{\phi}^2 \tilde{x} / 2} \right), \end{aligned} \quad (24b)$$

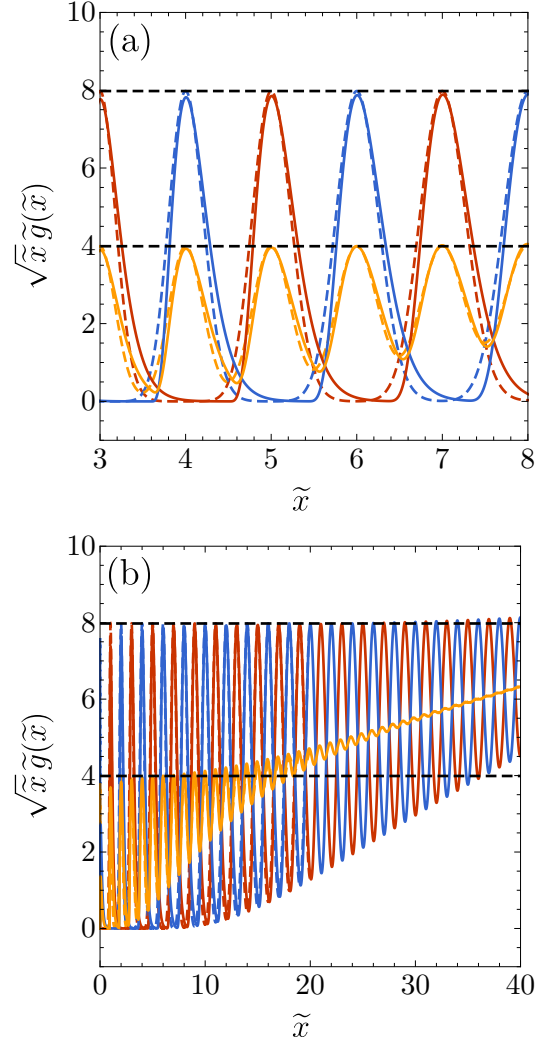


FIG. 4. Symmetric binary mixture with  $a = \frac{1}{2}$ . Plot of  $\sqrt{\tilde{x}} \tilde{g}_{11}(\tilde{x})$  (maxima at  $\tilde{x} \approx 1, 3, 5, \dots$ ),  $\sqrt{\tilde{x}} \tilde{g}_{12}(\tilde{x})$  (maxima at  $\tilde{x} \approx 0, 2, 4, \dots$ ), and  $\sqrt{\tilde{x}} \tilde{g}(\tilde{x})$  (maxima at  $\tilde{x} \approx 0, 1, 2, \dots$ ) for  $\phi = 0.9$ . Solid lines correspond to the exact functions, and dashed lines to our approximations [Eqs. (24)]. The horizontal dashed lines indicate  $2/\sqrt{2\pi\bar{\phi}^2} \simeq 7.98$  and  $1/\sqrt{2\pi\bar{\phi}^2} \simeq 3.99$ . Panel (a) shows  $3 \leq \tilde{x} \leq 8$ , and panel (b) shows  $0 \leq \tilde{x} \leq 40$ .

$$\begin{aligned} \tilde{g}(\tilde{x}) &= \frac{1}{2} [\tilde{g}_{11}(\tilde{x}) + \tilde{g}_{12}(\tilde{x})] \\ &\approx 1 + 2 \sum_{n=1}^{\infty} e^{-2n^2 \pi^2 \bar{\phi}^2 \tilde{x}} \cos(2n\pi \tilde{x}) \\ &= \theta_3 \left( \pi \tilde{x}, e^{-2\pi^2 \bar{\phi}^2 \tilde{x}} \right). \end{aligned} \quad (24c)$$

The corresponding envelopes are

$$\tilde{g}_{11}^{\text{env}}(\tilde{x}) = \tilde{g}_{12}^{\text{env}}(\tilde{x}) = \theta_3 \left( 0, e^{-\pi^2 \bar{\phi}^2 \tilde{x} / 2} \right), \quad (25a)$$

$$\tilde{g}^{\text{env}}(\tilde{x}) = \theta_3 \left( 0, e^{-2\pi^2 \bar{\phi}^2 \tilde{x}} \right). \quad (25b)$$

It is worth noting that only the even poles of  $\tilde{g}_{ij}(\tilde{x})$  contribute to the total RDF  $\tilde{g}(\tilde{x})$ . Consequently, while  $\tilde{g}_{11}(\tilde{x})$  and  $\tilde{g}_{12}(\tilde{x})$  have local maxima at  $\tilde{x} \approx 1, 3, 5, \dots$  and  $\tilde{x} \approx 0, 2, 4, \dots$ , respectively,  $\tilde{g}(\tilde{x})$  exhibits local maxima at  $\tilde{x} \approx 0, 1, 2, \dots$ . This reflects the near-close-packing particle arrangement of alternating types:  $1 - 2 - 1 - 2 - \dots$ . Equation (5) then implies

$$\tilde{g}_{ij}^{\text{env}}(\tilde{x}) \simeq \begin{cases} \frac{2}{\sqrt{2\pi\bar{\phi}^2\tilde{x}}}, & \tilde{x} \lesssim \frac{0.31}{\bar{\phi}^2}, \\ 1 + 2e^{-\pi^2\bar{\phi}^2\tilde{x}/2}, & \tilde{x} \gtrsim \frac{0.31}{\bar{\phi}^2}, \end{cases} \quad (26a)$$

$$\tilde{g}^{\text{env}}(\tilde{x}) \simeq \begin{cases} \frac{1}{\sqrt{2\pi\bar{\phi}^2\tilde{x}}}, & \tilde{x} \lesssim \frac{0.077}{\bar{\phi}^2} \\ 1 + 2e^{-2\pi^2\bar{\phi}^2\tilde{x}}, & \tilde{x} \gtrsim \frac{0.077}{\bar{\phi}^2}. \end{cases} \quad (26b)$$

The overall behavior of the total RDF  $\tilde{g}^{\text{env}}(\tilde{x})$  closely resembles that of the monocomponent system. However, the algebraic decay of the partial functions  $\tilde{g}_{ij}^{\text{env}}(\tilde{x})$  extends to distances four times larger than that of  $\tilde{g}^{\text{env}}(\tilde{x})$ .

The features described above are clearly illustrated in Fig. 4. In particular, the algebraic decay of the total RDF,  $\tilde{g}(\tilde{x}) \sim 1/\sqrt{\tilde{x}}$ , breaks down for  $\tilde{x} \gtrsim 10$ , whereas the algebraic decay of the partial functions,  $\tilde{g}_{ij}(\tilde{x})$ , persists up to  $\tilde{x} \gtrsim 40$ .

#### IV. EXTENSION TO CONFINED HARD DISKS

We now consider a q1D system of hard disks of unit diameter confined between two parallel lines. The disks are free to move along the longitudinal axis  $x$ , while their transverse positions are restricted to  $-\frac{\epsilon}{2} \leq y \leq \frac{\epsilon}{2}$ , where  $1 + \epsilon$  is the wall separation. For  $\epsilon \leq \frac{\sqrt{3}}{2}$ , each disk interacts only with its immediate left and right neighbors [8].

It can be shown that this q1D system of identical disks can be mapped onto a 1D polydisperse system of non-additive hard rods [9–12], which is considerably more complex than the binary mixture analyzed in Sec. III.

The longitudinal distance of two disks in contact, with transverse coordinates  $y$  and  $y'$ , is  $\sigma(y, y') = \sqrt{1 - (y - y')^2}$ , which ranges from  $\sigma(y, y) = 1$  to  $\sigma(\pm\frac{\epsilon}{2}, \mp\frac{\epsilon}{2}) = \sqrt{1 - \epsilon^2} \equiv a$ . The RDF,  $g(x; y, y')$ , thus depends on the longitudinal separation  $x$  and the transverse positions  $y$  and  $y'$  of both particles. The total RDF is obtained by averaging over all transverse positions:

$$g(x) = \int_{-\frac{\epsilon}{2}}^{\frac{\epsilon}{2}} dy f(y) \int_{-\frac{\epsilon}{2}}^{\frac{\epsilon}{2}} dy' f(y') g(x; y, y'), \quad (27)$$

where  $f(y)$  is the transverse probability distribution function.

As in Secs. II and III, we focus on the high-pressure behavior of  $g(x; y, y')$  and  $g(x)$  at sufficiently large longitudinal distances  $x$ . We first introduce the rescaled longitudinal distance as in Eq. (18). The choice of a single scaling value  $a = \sqrt{1 - \epsilon^2}$  is justified by the fact that, at high pressure, the disks tend to form a zigzag configuration, in which the longitudinal separation between neighboring disks is only slightly larger than  $a$ . This zigzag configuration is the analogue of the alternate arrangement  $1 - 2 - 1 - 2 - \dots$  in the 1D binary case. In the limit  $\beta p \gg 1$ , with  $p$  the longitudinal pressure, the equation of state becomes  $\beta p \approx 2\rho/(1 - \rho a)$  [9, 13], where  $\rho$  is the linear density. The divergence of  $\beta p$  as  $\rho \rightarrow 1/a$  motivates identifying the high-pressure packing fraction as  $\phi = \rho a$  in Eq. (18).

A careful numerical analysis of the poles of the Laplace transform of  $\tilde{g}(\tilde{x}; y, y') \equiv g(x; y, y')$  shows that, in the high-pressure limit,

$$\zeta_n \approx \frac{n^2 \pi^2 \bar{\phi}^2}{4}, \quad \omega_n \approx n\pi, \quad n = 1, 2, 3, \dots \quad (28)$$

Comparison with Eq. (21) reveals that, while the oscillation frequencies follow the same pattern as in the binary mixture, the damping coefficients are half the values of the binary system with the same  $\bar{\phi}$ . As in the factor 2 appearing in  $\beta p \approx 2\phi/\bar{\phi}$  [9, 13], this reduction arises from the effect of vertical fluctuations around the perfect zigzag configuration.

Near close packing, the dominant RDFs are

$$\tilde{g}_{++}(\tilde{x}) \equiv \tilde{g}\left(\tilde{x}; \frac{\epsilon}{2}, \frac{\epsilon}{2}\right) = \tilde{g}\left(\tilde{x}; -\frac{\epsilon}{2}, -\frac{\epsilon}{2}\right), \quad (29a)$$

$$\tilde{g}_{+-}(\tilde{x}) \equiv \tilde{g}\left(\tilde{x}; \frac{\epsilon}{2}, -\frac{\epsilon}{2}\right) = \tilde{g}\left(\tilde{x}; -\frac{\epsilon}{2}, \frac{\epsilon}{2}\right), \quad (29b)$$

so that

$$\tilde{g}(\tilde{x}) \approx \frac{1}{2} [\tilde{g}_{++}(\tilde{x}) + \tilde{g}_{+-}(\tilde{x})]. \quad (30)$$

Analogously to the binary case for  $\tilde{g}_{11}(\tilde{x})$  [Eq. (23a)], the residues of the Laplace transform of  $\tilde{g}_{++}(\tilde{x})$  alternate in sign.

In summary, for  $\bar{\phi} \ll 1$  we have

$$\tilde{g}_{++}(\tilde{x}) \approx \theta_3\left(\frac{\pi(\tilde{x} - 1)}{2}, e^{-\pi^2\bar{\phi}^2\tilde{x}/4}\right), \quad (31a)$$

$$\tilde{g}_{+-}(\tilde{x}) \approx \theta_3\left(\frac{\pi\tilde{x}}{2}, e^{-\pi^2\bar{\phi}^2\tilde{x}/4}\right), \quad (31b)$$

$$\tilde{g}(\tilde{x}) \approx \theta_3\left(\pi\tilde{x}, e^{-\pi^2\bar{\phi}^2\tilde{x}}\right). \quad (31c)$$

The corresponding envelopes are

$$\tilde{g}_{++}^{\text{env}}(\tilde{x}) = \tilde{g}_{+-}^{\text{env}}(\tilde{x}) = \theta_3\left(0, e^{-\pi^2\bar{\phi}^2\tilde{x}/4}\right), \quad (32a)$$

$$\tilde{g}^{\text{env}}(\tilde{x}) = \theta_3\left(0, e^{-\pi^2 \bar{\phi}^2 \tilde{x}}\right). \quad (32b)$$

As a consequence,

$$\tilde{g}_{++}^{\text{env}}(\tilde{x}) \simeq \begin{cases} \frac{2}{\sqrt{\pi \bar{\phi}^2 \tilde{x}}}, & \tilde{x} \lesssim \frac{0.62}{\bar{\phi}^2}, \\ 1 + 2e^{-\pi^2 \bar{\phi}^2 \tilde{x}/4}, & \tilde{x} \gtrsim \frac{0.62}{\bar{\phi}^2}, \end{cases} \quad (33a)$$

$$\tilde{g}^{\text{env}}(\tilde{x}) \simeq \begin{cases} \frac{1}{\sqrt{\pi \bar{\phi}^2 \tilde{x}}}, & \tilde{x} \lesssim \frac{0.15}{\bar{\phi}^2} \\ 1 + 2e^{-\pi^2 \bar{\phi}^2 \tilde{x}}, & \tilde{x} \gtrsim \frac{0.15}{\bar{\phi}^2}. \end{cases} \quad (33b)$$

Figure 5 demonstrates the good agreement between the exact distributions  $\tilde{g}_{++}(\tilde{x})$ ,  $\tilde{g}_{+-}(\tilde{x})$ , and  $\tilde{g}(\tilde{x})$  and our theoretical predictions, Eqs. (31). Comparison with Fig. 4 shows that the regime of intermediate algebraic decay extends over a wider range for confined disks than for the binary mixture with the same  $\phi$  and  $a$ . We also note that the agreement between the total RDF  $\tilde{g}(\tilde{x})$  and its approximation is slightly less accurate in the q1D confined disk system than in the 1D binary mixture, which is expected since Eq. (30) introduces an additional approximation in the q1D case.

The intermediate algebraic decay  $g^{\text{env}}(x) \sim 1/\sqrt{x}$  for confined disks was previously estimated in Ref. [7], improving upon the earlier decay law  $g^{\text{env}}(x) \sim x^{-2/3}$  proposed from computer simulations in Ref. [14]. Hu and Charbonneau (HC) justified their result by starting from the 1D algebraic decay [Eq. (6)], which in terms of pressure reads  $g^{\text{env}}(x) \simeq (1 + \beta p)^{3/2} / \sqrt{2\pi\beta p(x-1)}$ . They then made the substitutions  $\beta p \rightarrow \beta p a$  and  $x \rightarrow x/a$ , and introduced a correction factor  $c$ , obtaining

$$g_{\text{HC}}^{\text{env}}(x) \simeq c \frac{(1 + \beta p a)^{3/2}}{\sqrt{2\pi\beta p a(x/a - 1)}}. \quad (34)$$

By fitting data obtained via the planting method, they estimated  $c = 0.7$ . Using  $\beta p a \simeq 2\phi/\bar{\phi}$  and the scaled distance in Eq. (18), Eq. (34) can be rewritten as

$$\tilde{g}_{\text{HC}}^{\text{env}}(\tilde{x}) \simeq c \sqrt{2} \frac{(1 - \bar{\phi}/2)^{3/2}}{\sqrt{\pi \bar{\phi}^2 \tilde{x}}}. \quad (35)$$

Setting  $1 - \bar{\phi}/2 \simeq 1$  and choosing  $c = 1/\sqrt{2} \simeq 0.707$ , Eq. (35) exactly reproduces our result in Eq. (33b). Thus, our approach removes the need for empirical fitting entirely.

## V. CONCLUSIONS

We have presented an alternative derivation of the asymptotic behavior of the RDF in the Tonks gas at high

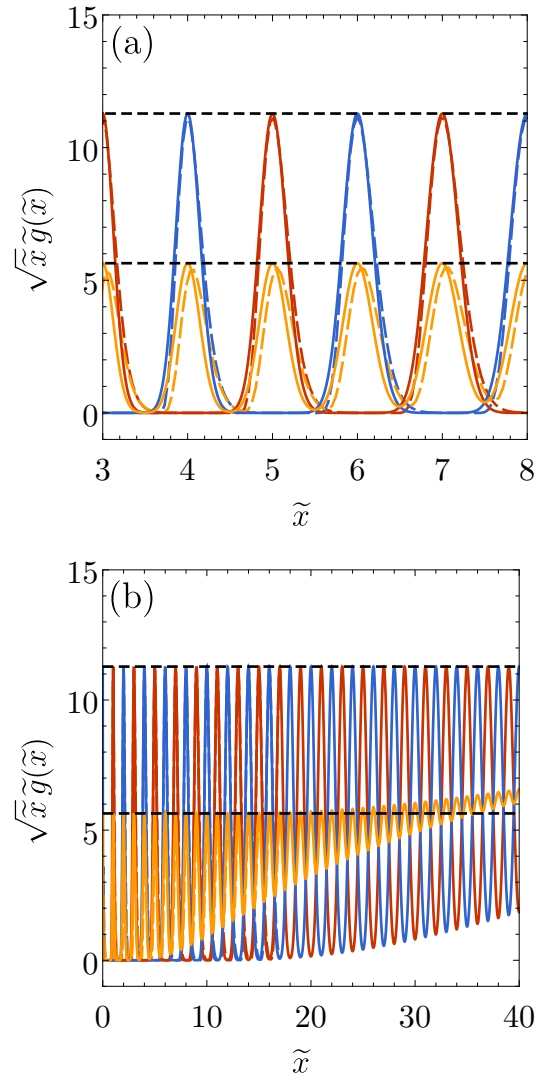


FIG. 5. Confined hard disks with  $\epsilon = \frac{\sqrt{3}}{2}$ . Plot of  $\sqrt{\tilde{x}}\tilde{g}_{++}(\tilde{x})$  (maxima at  $\tilde{x} \approx 1, 3, 5, \dots$ ),  $\sqrt{\tilde{x}}\tilde{g}_{+-}(\tilde{x})$  (maxima at  $\tilde{x} \approx 0, 2, 4, \dots$ ), and  $\sqrt{\tilde{x}}\tilde{g}(\tilde{x})$  (maxima at  $\tilde{x} \approx 0, 1, 2, \dots$ ) for  $\phi = 0.9$ . Solid lines correspond to the exact functions, and dashed lines to our approximations [Eqs. (31)]. The horizontal dashed lines indicate  $2/\sqrt{\pi\bar{\phi}^2} \simeq 11.28$  and  $1/\sqrt{\pi\bar{\phi}^2} \simeq 5.64$ . Panel (a) shows  $3 \leq \tilde{x} \leq 8$ , and panel (b) shows  $0 \leq \tilde{x} \leq 40$ .

packing fractions, based on Laplace transform techniques and pole analysis. Our approach yields a compact representation in terms of the Jacobi theta function  $\theta_3$  [6, 15], equivalent to the Gaussian superposition found by Bouzar and Messina [1], as demonstrated through the Poisson summation formula.

The representations in Eqs. (2) and (15) complement each other. While Eq. (2) approximates  $\tilde{g}(\tilde{x})$  as a superposition of Gaussian functions localized at  $\tilde{x} = n$ , Eq. (15) expresses  $\tilde{g}(\tilde{x})$  as a superposition of extended damped oscillatory modes. Beyond offering a more compact mathematical form, the Laplace-pole representation provides direct physical insight by connect-

TABLE I. Summary and comparison of the main results obtained in this work for the Tonks gas, the symmetric nonadditive binary mixture, and confined hard disks. The table compiles the scaling definitions, pole locations, theta-function forms of the RDFs and their envelopes, and the associated algebraic and exponential asymptotic behaviors in the high-packing-fraction limit.

Property	Tonks gas	Binary mixture	Confined hard disks
$\phi$	$\rho$	$\rho a$	$\rho a, \quad a = \sqrt{1 - \epsilon^2}$
$\tilde{x}$	$(x - 1)\phi$	$\left(\frac{x}{a} - 1\right)\phi$	$\left(\frac{x}{a} - 1\right)\phi$
$\zeta_n$	$2n^2\pi^2\bar{\phi}^2$	$\frac{n^2\pi^2\bar{\phi}^2}{2}$	$\frac{n^2\pi^2\bar{\phi}^2}{4}$
$\omega_n$	$2n\pi$	$n\pi$	$n\pi$
$\tilde{g}(\tilde{x})$	$\theta_3\left(\pi\tilde{x}, e^{-2\pi^2\bar{\phi}^2\tilde{x}}\right)$	$\theta_3\left(\pi\tilde{x}, e^{-2\pi^2\bar{\phi}^2\tilde{x}}\right)$	$\theta_3\left(\pi\tilde{x}, e^{-\pi^2\bar{\phi}^2\tilde{x}}\right)$
$\tilde{g}^{\text{env}}(\tilde{x})$	$\theta_3\left(0, e^{-2\pi^2\bar{\phi}^2\tilde{x}}\right)$	$\theta_3\left(0, e^{-2\pi^2\bar{\phi}^2\tilde{x}}\right)$	$\theta_3\left(0, e^{-\pi^2\bar{\phi}^2\tilde{x}}\right)$
Algebraic decay of $\tilde{g}^{\text{env}}(\tilde{x})$	$\frac{1}{\sqrt{2\pi\bar{\phi}^2\tilde{x}}}, \quad \tilde{x} \lesssim \frac{0.077}{\bar{\phi}^2}$	$\frac{1}{\sqrt{2\pi\bar{\phi}^2\tilde{x}}}, \quad \tilde{x} \lesssim \frac{0.077}{\bar{\phi}^2}$	$\frac{1}{\sqrt{\pi\bar{\phi}^2\tilde{x}}}, \quad \tilde{x} \lesssim \frac{0.15}{\bar{\phi}^2}$
Exponential decay of $\tilde{g}^{\text{env}}(\tilde{x}) - 1$	$2e^{-2\pi^2\bar{\phi}^2\tilde{x}}, \quad \tilde{x} \gtrsim \frac{0.077}{\bar{\phi}^2}$	$2e^{-2\pi^2\bar{\phi}^2\tilde{x}}, \quad \tilde{x} \gtrsim \frac{0.077}{\bar{\phi}^2}$	$2e^{-\pi^2\bar{\phi}^2\tilde{x}}, \quad \tilde{x} \gtrsim \frac{0.15}{\bar{\phi}^2}$
$\tilde{g}_{11}(\tilde{x}), \quad \tilde{g}_{++}(\tilde{x})$	—	$\theta_3\left(\frac{\pi(\tilde{x}-1)}{2}, e^{-\pi^2\bar{\phi}^2\tilde{x}/2}\right)$	$\theta_3\left(\frac{\pi(\tilde{x}-1)}{2}, e^{-\pi^2\bar{\phi}^2\tilde{x}/4}\right)$
$\tilde{g}_{12}(\tilde{x}), \quad \tilde{g}_{+-}(\tilde{x})$	—	$\theta_3\left(\frac{\pi\tilde{x}}{2}, e^{-\pi^2\bar{\phi}^2\tilde{x}/2}\right)$	$\theta_3\left(\frac{\pi\tilde{x}}{2}, e^{-\pi^2\bar{\phi}^2\tilde{x}/4}\right)$
$\tilde{g}_{ij}^{\text{env}}(\tilde{x})$	—	$\theta_3\left(0, e^{-\pi^2\bar{\phi}^2\tilde{x}/2}\right)$	$\theta_3\left(0, e^{-\pi^2\bar{\phi}^2\tilde{x}/4}\right)$
Algebraic decay of $\tilde{g}_{ij}^{\text{env}}(\tilde{x})$	—	$\frac{2}{\sqrt{2\pi\bar{\phi}^2\tilde{x}}}, \quad \tilde{x} \lesssim \frac{0.31}{\bar{\phi}^2}$	$\frac{2}{\sqrt{\pi\bar{\phi}^2\tilde{x}}}, \quad \tilde{x} \lesssim \frac{0.62}{\bar{\phi}^2}$
Exponential decay of $\tilde{g}_{ij}^{\text{env}}(\tilde{x}) - 1$	—	$2e^{-\pi^2\bar{\phi}^2\tilde{x}/2}, \quad \tilde{x} \gtrsim \frac{0.31}{\bar{\phi}^2}$	$2e^{-\pi^2\bar{\phi}^2\tilde{x}/4}, \quad \tilde{x} \gtrsim \frac{0.62}{\bar{\phi}^2}$

ing spatial correlations to the structure of the poles in Laplace space.

We have extended this framework to 1D binary mixtures and to q1D confined hard-disk systems, where the Laplace representation remains tractable and provides clear advantages over direct spatial decompositions. A synoptic comparison of the three systems—Tonks gas, binary mixture, and confined disks—is provided in Table I, highlighting the common structure of the poles and the corresponding algebraic regimes.

The pole structure obtained in the high-pressure limit reveals that the decay rates follow  $\zeta_n \propto n^2\bar{\phi}^2$  for  $\bar{\phi} \ll 1$  in all systems considered, a signature of the increasingly ordered (quasi-crystalline) arrangements near close packing. The associated oscillation frequencies establish the spatial periodicity of the underlying configurations.

Finally, the connection between spatial oscillations and pole structure may be useful for future studies of dynamical properties. Time-dependent correlation and response functions in confined geometries can be analyzed with similar Laplace-pole techniques, with the poles governing both spatial and temporal decay. The present framework thus provides a foundation for ex-

ploring dynamics in strongly correlated 1D and q1D fluids.

#### Appendix A: Laplace transforms for symmetric nonadditive binary mixtures

The Laplace transforms of  $g_{ij}(x)$  are [3]

$$G_{11}(s) = G_{22}(s) = \frac{2}{\rho} \frac{1 - Q_{11}(s) - D(s)}{D(s)}, \quad (\text{A1a})$$

$$G_{12}(s) = \frac{2}{\rho} \frac{Q_{12}(s)}{D(s)}, \quad (\text{A1b})$$

where

$$Q_{11}(s) = Q_{22}(s) = \frac{\beta p}{s + \beta p} \frac{e^{-s}}{1 + e^{(1-a)\beta p}}, \quad (\text{A2a})$$

$$Q_{12}(s) = \frac{\beta p}{s + \beta p} \frac{e^{-as}}{1 + e^{-(1-a)\beta p}}, \quad (\text{A2b})$$

$$D(s) = \left[ 1 - \frac{\beta p}{s + \beta p} \frac{e^{-s}}{1 + e^{(1-a)\beta p}} \right]^2 - \left[ \frac{\beta p}{s + \beta p} \frac{e^{-as}}{1 + e^{(1-a)\beta p}} \right]^2. \quad (\text{A2c})$$

In the high-pressure regime ( $\beta p \gg 1$ ),

$$Q_{11}(s) \approx 0, \quad Q_{12}(s) \approx \left( 1 + \frac{a\bar{\phi}s}{\phi} \right)^{-1} e^{-as}, \quad (\text{A3a})$$

$$D(s) \approx \frac{1 + \frac{a\bar{\phi}}{\phi}s - e^{-as}}{1 + \frac{a\bar{\phi}}{\phi}s} \frac{1 + \frac{a\bar{\phi}}{\phi}s + e^{-as}}{1 + \frac{a\bar{\phi}}{\phi}s}. \quad (\text{A3b})$$

## ACKNOWLEDGMENTS

The authors acknowledge financial support from Grant No. PID2024-156352NB-I00 funded by MCIU/AEI/10.13039/501100011033/FEDER, UE and from Grant No. GR24022 funded by the Junta de Extremadura (Spain) and by European Regional Development Fund (ERDF) "A way of making Europe." A.M.M. is grateful to the Spanish Ministerio de Ciencia e Innovación for a fellowship PRE2021-097702.

## DATA AVAILABILITY

Data supporting figures and numerical results are available from the corresponding author upon reasonable request.

- 
- [1] L. Bouzar and R. Messina, Emerging crystallization in one dimension, *Phys. Rev. E* **112**, L042105 (2025).
- [2] L. Tonks, The complete equation of state of one, two and three-dimensional gases of hard elastic spheres, *Phys. Rev.* **50**, 955 (1936).
- [3] A. Santos, *A Concise Course on the Theory of Classical Liquids. Basics and Selected Topics*, Lecture Notes in Physics, Vol. 923 (Springer, New York, 2016).
- [4] A. M. Montero and A. Santos, Exploring anisotropic pressure and spatial correlations in strongly confined hard-disk fluids. Exact results, *Phys. Rev. E* **110**, L022601 (2024).
- [5] A. M. Montero and A. Santos, Exact anisotropic properties of hard spheres in narrow cylindrical confinement, *J. Chem. Phys.* **163**, 024506 (2025).
- [6] NIST Digital Library of Mathematical Functions, <https://dlmf.nist.gov/>, Release 1.2.4 of 2025-03-15, F. W. J. Olver, A. B. Olde Daalhuis, D. W. Lozier, B. I. Schneider, R. F. Boisvert, C. W. Clark, B. R. Miller, B. V. Saunders, H. S. Cohl, and M. A. McClain, eds.
- [7] Y. Hu and P. Charbonneau, Comment on "Kosterlitz-Thouless-type caging-uncaging transition in a quasi-one-dimensional hard disk system", *Phys. Rev. Res.* **3**, 038001 (2021).
- [8] D. A. Kofke and A. J. Post, Hard particles in narrow pores. Transfer-matrix solution and the periodic narrow box, *J. Chem. Phys.* **98**, 4853 (1993).
- [9] A. M. Montero and A. Santos, Equation of state of hard-disk fluids under single-file confinement, *J. Chem. Phys.* **158**, 154501 (2023).
- [10] A. M. Montero and A. Santos, Structural properties of hard-disk fluids under single-file confinement, *J. Chem. Phys.* **159**, 034503 (2023).
- [11] A. M. Montero and A. Santos, Exact equilibrium properties of square-well and square-shoulder disks in single-file confinement, *Phys. Rev. E* **110**, 024601 (2024).
- [12] A. M. Montero, *Equilibrium properties of strongly confined fluids*, Ph.D. thesis, University of Extremadura (2025).
- [13] S. Varga, G. Balló, and P. Gurin, Structural properties of hard disks in a narrow tube, *J. Stat. Mech.* **2011**, P11006 (2011).
- [14] A. Huerta, T. Bryk, V. M. Pergamenschik, and A. Trokhymchuk, Kosterlitz-Thouless-type caging-uncaging transition in a quasi-one-dimensional hard disk system, *Phys. Rev. Res.* **2**, 033351 (2020).
- [15] Wolfram Research, Inc., *Mathematica* (2025).